Science of the Total Environment 979 (2025) 179464

Contents lists available at ScienceDirect

Science of the Total Environment

journal homepage: www.elsevier.com/locate/scitotenv

Investigating ozone build-up in the east of England during the July 2015 heat wave

Johana Romero-Alvarez [a,b,*], Aurelia Lupaşcu [c,f], Steve Dorling [d], Claire E. Reeves [d], Tim Butler [c,e]

[a] Cooperative Institute for Research in Environmental Sciences, University of Colorado Boulder, Boulder, USA
[b] NOAA Global Systems Laboratory, Boulder, USA
[c] Research Institute for Sustainability - Helmholtz Centre Potsdam, Germany
[d] School of Environmental Sciences, University of East Anglia, Norwich, UK
[e] Freie Universität Berlin, Institut für Meteorologie, Berlin, Germany
[f] European Centre for Medium-Range Weather Forecasts, Bonn, Germany

HIGHLIGHTS

- O_3-tagging in WRF-Chem quantifies NO_x contributions to the observed O_3 build-up
- SE winds brought O_3 from Western EU (60 %), while UK NO_x contributed 4.6 %
- Domestic sources had a greater impact on surface O_3 during south-southwesterly flows

GRAPHICAL ABSTRACT

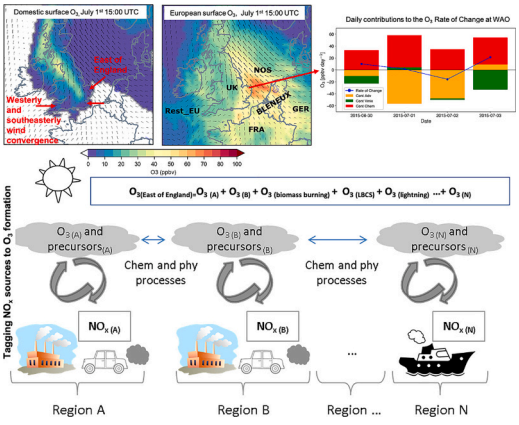

ARTICLE INFO

Editor: Hai Guo

Keywords:
Transboundary pollution
Domestic emissions
Ozone-tagging
In-situ photochemical production
Morning boundary layer mixing
Regional collaboration policies

ABSTRACT

Ozone (O_3) precursors controls have reduced peak episodes in the UK, yet some regions still exceed the 50 ppbv (8-h) limit under certain meteorological conditions. This study uses O_3-tagging within WRF-Chem to quantify NO_x contributions to near-surface O_3 across the East of England during a short heatwave (30 June–5 July 2015), where O_3 peaked at 116 ppbv. Despite underestimating peak O_3, the model effectively captures the episode's evolution and spatial extent (MB: −2 ppbv, r: 0.78), depicting O_3 increases on the hottest days and their decline. During the peak O_3 event, Western Europe contributed ~60 % of daily mean O_3, while domestic NO_x emissions accounted for only ~4.6 %. South-easterly winds transported O_3 and precursors from BENELUX, France, Germany, the North Sea, and the English Channel. Near-surface wind convergence (−0.00002 s^{-1}) with weaker

* Corresponding author at: Cooperative Institute for Research in Environmental Sciences, University of Colorado Boulder, Boulder, USA.
E-mail address: lero1992@colorado.edu (J. Romero-Alvarez).

https://doi.org/10.1016/j.scitotenv.2025.179464
Received 17 December 2024; Received in revised form 14 April 2025; Accepted 15 April 2025
Available online 22 April 2025

westerlies redirected domestic O_3 to the central UK, intensifying continental influence. Conversely, south-southwesterly flows amplified domestic O_3 contributions.

Analysis of the processes contributing to O_3 build-up highlights that transboundary transport played a significant role during the peak event. Boundary layer growth contributed by entraining O_3-rich air (up to 10.3 ppb h^{-1} across the boundary layer top), along with precursors from the residual layer, facilitating their downward mixing to surface levels. This process set the stage for in-situ photochemical O_3 production, which peaked at midday, contributing to a total daily O_3 production of 42 ppbv on average across the region. Our findings underscore the necessity of coordinated international efforts to manage transboundary pollution, alongside targeted local measures to reduce O_3 precursor emissions.

1. Introduction

Tropospheric ozone (O_3) is a secondary trace gas of significant atmospheric importance, acting both as a key oxidant and a harmful pollutant, posing risks to human health, crops, and ecosystems (Fuhrer, 2009; WHO, 2016). It primarily forms through a non-linear process initiated by the reaction of nitric oxide (NO) with the hydroperoxyl radical (HO_2), producing nitrogen dioxide (NO_2). HO_2 itself is generated when Non-Methane Volatile Organic Compounds (NMVOCs) react with hydroxyl radicals (OH). Subsequent photolysis of NO_2 ultimately yields O_3 (Monks, 2005). Tropospheric O_3 formation is critically dependent on the availability of nitrogen oxides ($NO_x = NO + NO_2$) and NMVOCs (Atkinson, 2000).

Clear skies, high temperatures, light winds, and low humidity associated with summertime anticyclonic conditions frequently trigger photochemical O_3 episodes across Europe and the UK (Ordóñez et al., 2017; Otero et al., 2016; Otero et al., 2022; Pope et al., 2016; Porter et al., 2015; Pusede et al., 2015; Jacob and Winner, 2009). Over 30 % of European summer days experiencing high-latitude blocking patterns, persistent anticyclonic systems often linked to heatwaves, coincide with O_3 exceedances above the 90th percentile. These conditions increase the likelihood of simultaneous extreme O_3 concentrations and temperature exceedances by 15 %–20 % (e.g., Ordóñez et al., 2017; Matsueda, 2011; Otero et al., 2022).

Chemical transport models (CTMs) have been used to explore this O_3-temperature relationship and demonstrate that anticyclonic conditions reduce cloud formation and limit pollutant dispersion, causing the accumulation of O_3 precursors. Increased solar radiation and higher maximum temperatures accelerate photolysis and enhance VOC emissions, particularly those from biogenic sources (Vieno et al., 2010). Additionally, prolonged heat dries soils, triggering positive feedback that further elevates temperatures. Concurrently, stomatal closure in plants reduces O_3 uptake, increasing surface O_3 concentrations (Solberg et al., 2008; Vieno et al., 2010; Grünhage et al., 2012). Recent advancements in CTMs, including source attribution techniques, have improved our understanding of how meteorological conditions, particularly shifts in circulation patterns, alter precursor contributions to O_3 formation during peak pollution episodes (Butler et al., 2018; Butler et al., 2020a, 2020b; Grewe et al., 2017; Mertens et al., 2020; Romero-Alvarez et al., 2022).

Despite stricter UK and European regulations have reduced primary O_3 precursor emissions over the past 30 years, episodes of high O_3 can still happen, particularly in the East of England. Here, concentrations can exceed the national objective of 50 ppbv (8-h average), typically at temperatures above 18 °C (AQEG, 2009; Derwent et al., 2018; Finch and Palmer, 2020). Severe O_3 episodes, with mixing ratios exceeding 90 ppbv, frequently occur when temperatures surpass 28–30 °C, often linked to polluted air transported from mainland Europe under anticyclonic conditions (Jenkin et al., 2002; Pope et al., 2016; Lee et al., 2006). A notable event occurred in 2003, when anticyclonic circulation over northern France led to temperature anomalies of 6–7 °C in the UK, causing repeated exceedances of the European Maximum Daily 8-h Average (MDA8) O_3 threshold of 120 μg m^{-3} (~60 ppbv) in Southeast England (Garcia-Herrera et al., 2010; Lee et al., 2006).

During the summer of 2015, persistent blocking conditions from late June to mid-September across Central and Western Europe led to multiple heat episodes (Hoy et al., 2017; Ionita et al., 2017; CAMS, 2016; DEFRA, 2017; Lupaşcu et al., 2022). This heat event, ranked sixth in severity since 1950, with the 2003 heatwave ranked second (Russo et al., 2015), featured a notable O_3 episode from June 30th to July 4th with O_3 mixing ratios in the UK exceeding the EU information threshold of 1-h average mixing ratio of 90 ppbv (180 μg m^{-3}). This episode coincided with the ICOZA field campaign at the Weybourne Atmospheric Observatory (WAO) on the North Norfolk Coast in the East of England, on tropospheric O_3 chemistry (Crilley et al., 2018). During this period, south-easterly winds led to surface O_3 mixing ratios reaching 116 ppbv, which is unusually high given past reductions in precursor emissions (AQEG, 2009; Finch and Palmer, 2020).

Since 2015, elevated O_3 levels and high temperatures have been recorded across Europe and the UK, with significant mortality linked to extreme heat during the summers of 2018, 2019, 2020, and 2022 (e.g., Rousi et al., 2023; Rustemeyer and Howells, 2021; Thompson et al., 2022). As global temperatures continue to rise, climate change is expected to increase the frequency of heatwaves and associated high O_3 episodes (Russo et al., 2015; Jacob and Winner, 2009). For example, rural sites such as the WAO are projected to exceed the moderate health threshold of 100 μg $m^{-3(\sim 50\ ppbv)}$ > 25 times per year (Gouldsbrough et al., 2022). Given these trends, understanding the factors driving O_3 build-up is essential for cross-border management and public health protection.

This study employs an O_3-tagging mechanism within the WRF-Chem model to quantify the contribution of NO_x emissions from different European regions to surface O_3 levels in East England during a heatwave event. Additionally, O_3 tendencies are analyzed to characterize the chemical and meteorological mechanisms influencing O_3 accumulation. Observational data collected during the ICOZA campaign provide a benchmark to describe the meteorological and chemical conditions experienced during the pollution episode and to evaluate model performance.

Section 2 details the model setup and methodology used to investigate O_3 sources during the build-up phase. Section 3 presents observed conditions during the ICOZA campaign, model evaluation results, and insights from applying the O_3-tagging method. Section 4 summarizes the main findings and discusses their broader implications.

2. Methods

2.1. WRF-Chem setup

We used the Weather Research and Forecasting model (WRF) version 3.7.1 (Powers et al., 2017) with chemistry (WRF-Chem) (Grell et al., 2005). The model domain was centred at 3° E and 53° N, covering most of Europe, as shown in Fig. 1. The spatial resolution was set to 27 km × 27 km, with 35 vertical levels starting from the surface up to 10 hPa. This resolution was chosen to balance computational efficiency and the source region representation while covering a sufficiently large domain for long-range transport. Uncertainties in local O_3 chemistry and small-scale transport should be considered when interpreting the results. The

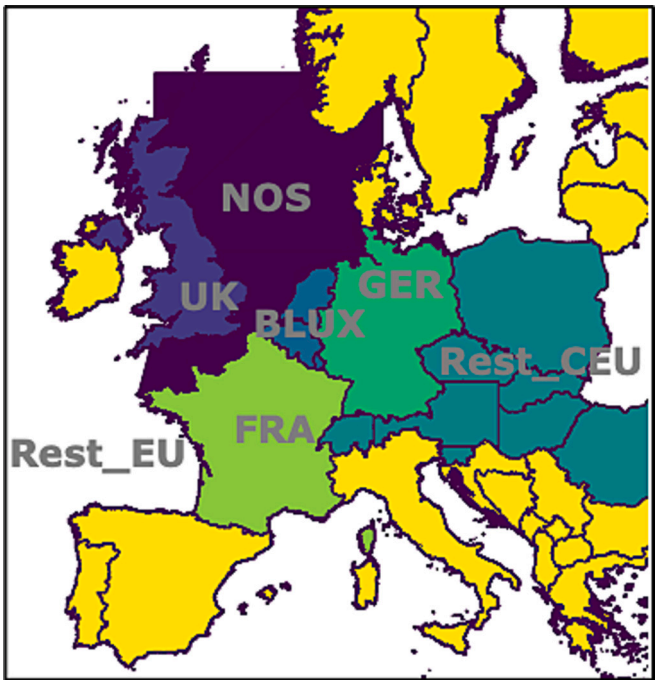

Fig. 1. Emission source regions. The Rest_EU region includes ship emissions from the Atlantic, the Mediterranean, the Baltic Sea, and the land areas in yellow. BLUX refers to BENELUX and the black line indicates the tagged LBCs.

initial and lateral boundary conditions (ICs and LBCs, respectively) for meteorology were obtained from the ERA-Interim reanalysis dataset (Dee et al., 2011) which has a spatial grid resolution of 0.75° × 0.75° and 6-h temporal resolution. ICs and LBCs for the chemistry fields were obtained from global simulations produced using the Chemistry Transport Model for O_3 and Related Chemical Tracers MOZART-4 GEOS-5 (Emmons et al., 2012) at three hourly intervals. The schemes used to parameterize the atmospheric processes are those deployed in Romero-Alvarez et al. (2022).

Simulations were conducted between June 30th and July 31st 2015 for gas-phase chemistry using a tagged-ozone mechanism based on the MOZART-4 chemical scheme. Anthropogenic emissions of carbon monoxide (CO), NO_x, sulphur dioxide (SO_2), and total NMVOCs for the European domain, including shipping routes, were taken from the TNO-MACC-III European inventory (Kuenen et al., 2014) for the year 2011. The emissions were provided as yearly totals (kg yr^{-1}) by source sector following the SNAP (selected nomenclature for sources of air pollution) convention at a 0.125° × 0.0625° longitude-latitude resolution.

Reported NO_2/NO_x emission ratios vary widely in the literature, ranging from lower estimates (e.g., 5.3 % by Liu et al. (2017)) to substantially higher values (e.g., 39 % by Richmond-Bryant et al. (2017)). In this study, a split of 95 % NO and 5 % NO_2 is applied. Emissions are also temporally disaggregated to account for monthly, weekly, and hourly variations based on the SNAP sector classification, following the methodology of Van Der Gon et al. (2011).

We note that the use of the TNO-MACC-III emissions inventory may not fully capture emission reductions that occurred between 2011 and 2015, with NO_x and NMVOC emissions in Europe and the UK decreasing by approximately 20 % and 14 %, respectively, for all sectors (Kuenen et al., 2022). Despite this, our findings remain relevant for regional O_3 analysis given the model's spatial resolution. However, uncertainties regarding the representativeness of emission trends should be considered when interpreting the results.

For the UK domain, emissions were taken from the UK National Emissions Inventory (NAEI) 2014, http://naei.beis.gov.uk/, with a spatial resolution of 1 km × 1 km. Biogenic emissions were calculated online using the Model of Emissions of Gases and Aerosols from Nature (MEGAN) version V2.04.

2.2. Ozone tagging mechanism

The present study employs the O_3 tagging method described in Romero-Alvarez et al. (2022), which is based on the approach proposed by Butler et al. (2018) and Lupaşcu and Butler (2019). This tagging technique labels O_3 molecules based on their origin, enabling the attribution of O_3 mixing ratios in a receptor area to their geographic sources. It assigns O_3 to its precursors according to its formation source rather than its instantaneous net production or destruction. Consequently, total source contributions remain positive even during periods of net O_3 loss, such as night-time NO titration (Butler et al., 2018). To achieve this, a modified chemical mechanism, "mozart_tag_kpp (chemopt = 113)", was implemented into WRF-Chem. This mechanism is based on MOZART-4 with added tracers to track the contributions from designated regions. The tagged-ozone technique is preferred over the perturbation approach as it directly tracks the transformation of specific precursor emissions (here, NO_x) into the O_3 fromation, minimizing inaccuracies caused by the nonlinear nature of O_3 chemistry. In contrast, the perturbation approach can lead to misattributions, for example, Emmons et al. (2012) found that reducing NO emissions by 20 % resulted in an underestimation of O_3 contributions by a factor of four. Table 1 of Mertens et al. (2020) further highlights the differences between these approaches, comparing the scientific questions that can be addressed using perturbation methods versus source attribution techniques like tagging.

O_3 formation relies on both NO_x and peroxyl radicals derived from VOCs. Research by Butler et al. (2020a, 2020b) and Lupaşcu et al. (2022) indicates that anthropogenic NMVOC emissions have a limited effect on regional O_3 production, with methane and biogenic VOCs playing more substantial roles. Since this study is primarily focuses with the impact of anthropogenic sources on O_3, NO_x tagging is chosen as a practical approach for source attribution.

To determine contributions to surface O_3, the study domain is divided into three main regions, illustrated in Fig. 1: (1) the UK, encompassing England, Wales, Northern Ireland, and Scotland; (2) the lateral boundaries; and (3) Europe, which is further subdivided into six areas: France (FRA); BENELUX (Belgium, the Netherlands, and Luxembourg); Germany (GER); the North Sea and English Channel (NOS); the remainder of Central Europe (Rest_CEU), covering Austria, Switzerland, the Czech Republic, Hungary, Poland, Slovakia, Slovenia, and Romania; and the Rest of Europe (Rest_EU), which includes the Iberian Peninsula, Southern, South-eastern, Eastern, and Northern Europe, Ireland, and emissions from shipping routes in the Atlantic, Baltic Sea, and Mediterranean. This configuration enables us to differentiate contributions from Western and Central Europe and Europe's busiest shipping routes.

The East of England, located on the eastern coast and one of England's nine official regions, serves as the receptor area. This region's environmental relevance is heightened by its proximity to continental Europe and potential exposure to cross-border pollution.

Additionally, the physical and chemical processes influencing the evolution of modelled O_3 over time, such as advection (upward/downward, eastward/northward mass transfer), vertical mixing (including dry deposition and diffusion), and net chemical production, are output as diagnostics and used to assess their impacts on the rate of change in the total modelled O_3 (Wong, 2013). These tendencies are estimated for four sites in the East of England and are also derived for tagged O_3 originating from NO_x emissions from specific source regions.

To complement the analysis, we also estimated the hourly O_3 flux at the top of the Planetary Boundary Layer (PBL). This is defined as the product of the entrainment velocity and the difference in O_3 mixing ratios above and below the PBL, following the methodology described in (Kaser et al., 2017) in their WRF-Chem study over the Colorado Front Range. The altitudes above and below the PBL are determined by tracing

the hourly PBL growth rate and interpolating O_3 mixing ratios at the corresponding heights. Specifically, during the morning and afternoon (07:00 to 16:00 UTC), a positive PBL growth rate is expected. In this case, the above-PBL O_3 mixing ratio is extracted using the next hour's (h + 1) PBL height plus 125 m as a reference. This offset corresponds to the maximum average PBL growth rate modelled across all sites (125 m h^{-1}). Conversely, the below-PBL O_3 mixing ratio is retrieved using the previous hour's (h-1) PBL height.

For the remaining hours, when a negative PBL growth rate is expected, the above-PBL O_3 mixing ratio is extracted at the previous hour's (h-1) PBL height + 125 m, and the below-PBL O_3 mixing ratio is retrieved using the next hour's (h + 1) PBL height.

2.3. Model Evaluation

Romero-Alvarez et al. (2022) have extensively evaluated WRF-Chem's performance over the UK and Europe, assessing 2-m temperature, 10-m wind speed and direction, and chemical fields such as NO_x and O_3. Their study utilized the same tagging scheme and model settings described here for summer 2015, providing a relevant reference for model performance in a comparable setup. Their findings indicate that the model effectively represents the spatial distribution of MDA8 O_3 levels above 50 and 60 ppbv, with the highest frequency of such days occurring in East Anglia, in the East of England. However, the model tends to underestimate the number of days with MDA8 O_3 levels exceeding 50 ppbv in East Anglia, consistent with previous studies highlighting the difficulties faced by many chemical transport models in accurately simulating high O_3 mixing ratios during pollution events in the UK (Archer-Nicholls et al., 2014; Francis et al., 2011) and across Europe (Lupaşcu et al., 2022). In this study, we extend the model evaluation using hourly observations of 2-m temperature, wind speed and direction, CO, O_3, NO_x, and reactive nitrogen oxides (NO_y) collected from June 29th to August 1st during the ICOZA field campaign (Woodward-Massey et al., 2023; Crilley et al., 2018). ICOZA took place in June–July 2015 at WAO (52.95° N, 1.12° E), a Global Atmospheric Watch regional station operated by the University of East Anglia and supported by the National Centre for Atmospheric Science (https://weybourne.uea.ac.uk/). The site is located at 16 m above sea level, approximately 50 km northwest of Norwich and 190 km northeast of London. The nearest major road is a rural route situated around 800 m to the south. WAO is exposed to clean air masses traveling southward over the North Sea, originating from polar regions, as well as to more polluted air influenced by emissions from major UK cities such as London and Birmingham and continental Europe (Lee et al., 2009). Additionally, the site is affected by local road emissions and influences from shipping (Penkett et al., 1999). Statistical metrics, including mean bias (MB), root mean square error (RMSE) and the coefficient of determination (R^2), were employed to assess the model's performance.

3. Results and discussion

3.1. Meteorological and chemical conditions observed during ICOZA

Most of the campaign was dominated by westerly and south-westerly winds. Temperatures ranged from 9 to 29 °C, with an average of 16 °C (see Fig. S.1.1a). The highest daytime and night-time temperatures were recorded between June 30th and July 2nd, coinciding with the period of most elevated O_3 levels.

On June 30th, a broad area of high pressure centred over the Dutch coast affected most of England (Fig. S.1.2). At WAO, temperatures reached up to 24 °C, with light winds predominantly from the south-southeast (see Fig. S.1.1a and b). An increase in the O_3 mixing ratio of 16.6 ppbv h^{-1} was observed coinciding with a shift in wind direction from south-southwest to south-southeast (Figs. S.1.1b and d). A peak mixing ratio of 64 ppbv was recorded at noon. Overnight temperatures remained above 17 °C, and the O_3 mixing ratios decreased to 40 ppbv, remaining nearly constant until the following day. Time series from European Monitoring and Evaluation Programme (EMEP) sites indicate that O_3 levels also began to rise at other stations in the south-eastern UK and parts of Western Europe (Fig. S.1.3), suggesting that the O_3 build-up was a regional-scale phenomenon.

By midnight, the high-pressure system centre had moved to Denmark (Fig. S.1.2b), placing WAO under moderate winds fluctuating between east and southeast (see Fig. S.1.1b). On July 1st, O_3 mixing ratios began to increase, and by 11:00 UTC, WAO recorded an O_3 concentration increase of approximately 17 ppbv h^{-1}. This significant morning rise in O_3 mixing ratios has been similarly observed in other field campaigns in South East UK (Lee et al., 2006) and is attributed to both the mixing of O_3-rich air from the residual layer to the surface and photochemical production of O_3 throughout the troposphere (Entwistle et al., 1997; Lee et al., 2006; Francis et al., 2011).

The increase in morning O_3 mixing ratios was accompanied by a wind shift from east-southeast to southeast and a surface temperature rise of about 6 °C (see Figs. S.1.1a and b). During the same period, relative humidity dropped from 81 % at 10:00 UTC to 58 % and 39 % at 11:00 and 12:00 UTC, respectively, suggesting a change in the air mass (Fig. S.1.1c). A maximum O_3 mixing ratio of 78 ppbv was reached at 12:00 UTC. Temperatures rose to 29 °C by 13:00 UTC, and O_3 mixing ratios continued to increase throughout the afternoon, reaching 116 ppbv at 18:00 UTC. Meanwhile, record-breaking temperatures were also recorded in parts of Southeast England, including London Heathrow, which experienced its highest temperature since the August 2003 heatwave (36.7 °C) (WMO, 2016). Heat health alerts were in effect for Southeast England and East Anglia. The UK Met Office attributed these elevated temperatures to a southerly airflow originating from Spain, which was experiencing its longest recorded heatwave, from June 27 to July 22 (WMO, 2016). WAO surface O_3 peaked above the EU information threshold (see Fig. 2). This peak, recorded in the evening when photochemical O_3 production typically decreases as solar radiation weakens, suggests that the pollution event was likely due to O_3 transport. This is further supported by elevated CO mixing ratios recorded that day (Fig. 2b). NO and NO_2 mixing ratios were also elevated on the morning of July 1st, with a maximum NO mixing ratio of 3.4 ppbv at 10:00 UTC, nearly three times higher than the campaign average. NO_2 mixing ratios reached an exceptional morning peak of 9 ppbv at 10:00 UTC, more than four times the average campaign concentration. Comparison of modelled O_3 mixing ratios and temperature at four rural monitoring stations in eastern UK (Sibton, St Osyth, Wicken Fen, and WAO) (Fig. S.1.4. in the supplementary material) during July 1st (extreme heat period) and the rest of the campaign shows that both O_3 and temperature were significantly higher on July 1st compared to other days. The 5th and 95th percentiles whiskers show that both the highest and lowest O_3 and temperature values during the heat event exceeded the mean of the rest of the campaign. Moreover, the 90th percentile of O_3 mixing ratios increased respectively by 39 %, 32 %, 36 %, and 27 % at Sibton, St Osyth, Wicken Fen, and WAO on July 1st compared to the rest of the campaign, indicating a strong correlation between the high temperatures and elevated O_3 levels. While temperature affects several interrelated processes, such as photochemical reaction rates and biogenic VOC emissions production, a detailed attribution of the temperature contribution to the observed O_3 enhancements during the heatwave is beyond the scope of this study.

Rural stations in eastern UK (e.g., Wicken Fen, Sibton, St Osyth, and High Muffles) and south-eastern UK (e.g., Lillington Heath) also recorded O_3 levels exceeding the EU information threshold of a 1-h average of 180 μg m^{-3}. Similar mixing ratios were observed at sites in the Netherlands (e.g., de Zilk, Cabauw Wielsekade, and Vredepeel) and in Germany (e.g., Schauinsland) (see Fig. S.1.3). The episode ended following a shift in wind direction to southwest, bringing cooler and cleaner air from the Atlantic late on July 1st and early on July 2nd (see Fig. S.1.1b, c, and d). O_3 mixing ratios decreased by 14 ppbv between 12:00 and 13:00 UTC. Lower NO_x mixing ratios were observed the

following morning on July 2nd, with maximum NO mixing ratios below 1 ppbv and NO_2 near 2 ppbv (see Fig. S.1.1f and g). In the afternoon, an increase in O_3 mixing ratios (up to 6.7 ppbv h^{-1}) coincided with a wind direction shift from west-southwest to south-southeast. Background stations on the west coast of the Netherlands, such as de Zilk and Kollumerwaard, further indicate that O_3 reached mixing ratios as high as 100 ppbv on this day (see Fig. S.1.3). Regionally, the episode lasted several days, in the East of England O_3 mixing ratios fluctuate during the following 2 days without exceeding 60 ppbv.

3.2. Model performance

Fig. 3 compares modelled and observed temperature (°C), wind speed (m/s), and wind direction (degrees) at WAO from June 29th to July 31st, 2015. Table 1 presents the statistical metrics for these meteorological variables. The model tends to underestimate temperature, particularly in the early days of the campaign, with an average mean bias (MB) of −1.5 °C. This underestimation is expected given WAO's coastal location and the challenges of accurately modelling coastal dynamics, such as sea breezes, at a coarse resolution of 27 km (Steele et al., 2014). Romero-Alvarez et al. (2022) also show that the model configuration has difficulty capturing diurnal temperature variation near coastal sites across the UK and shows wind speed biases, with positive biases during southerly, easterly, and westerly winds and negative biases during northerly winds. Despite these limitations, Fig. 3b demonstrate a moderate agreement between observed and modelled wind speeds at WAO, with an MB of 0.09 m/s.

Fig. S.2.1, in the supplemental material, presents model validation for June 29th to July 31st, 2015, using a subset of observations from the ICOZA campaign (NO, NO_2, NO_x, NO_y, CO, and O_3) (Crilley et al., 2018; Woodward-Massey et al., 2023). Modelled NO_y includes contributions

Table 1
Summary of statistical comparisons between simulated and measured variables at WAO from June 29th to July 31st. MB units are the same as the parameter units.

Parameter/metric units	Mean Obs.	Mean model	RMSE	MB	r	R^2
Temperature (°C)	17.0	15.4	2.6	−1.5	0.81	0.28
Wind speed (m/s)	5.4	5.5	1.9	0.09	0.64	0.23
NO (ppbv)	0.40	0.35	0.4	−0.04	0.58	0.20
NO_2 (ppbv)	2.77	2.38	1.6	−0.39	0.60	0.19
NO_x (ppbv)	3.16	2.73	1.8	−0.43	0.60	0.20
NO_y (ppbv)	5.08	3.08	2.6	−2.0	0.65	0.46
CO (ppbv)	114.5	125.7	21.0	11.1	0.67	0.28
O_3 (ppbv)	35.8	33.5	9.5	−2.3	0.78	0.53

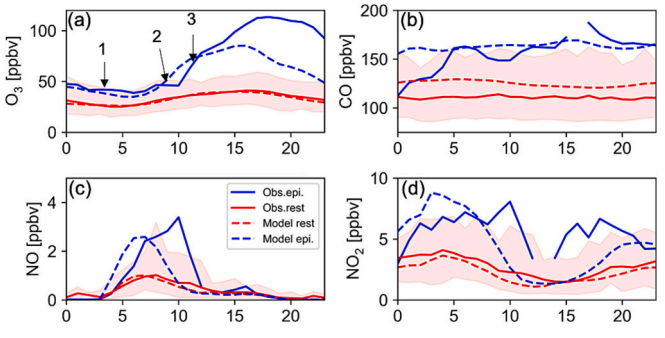

Fig. 2. Diurnal cycle of observed (solid line) and modelled (dashed line) (a) O_3, (b) CO, (c) NO, and (d) NO_2 during July 1st (blue line) and the average for the rest of the field campaign (red line). The shaded areas represent the variability in observations, showing the 25th and 75th percentiles. The numbers 1, 2, and 3 in panel (a) highlight changes in O_3 mixing ratios on July 1st, corresponding to periods when the observed wind predominantly came from the south-southeast, east-southeast, and south-southeast, respectively.

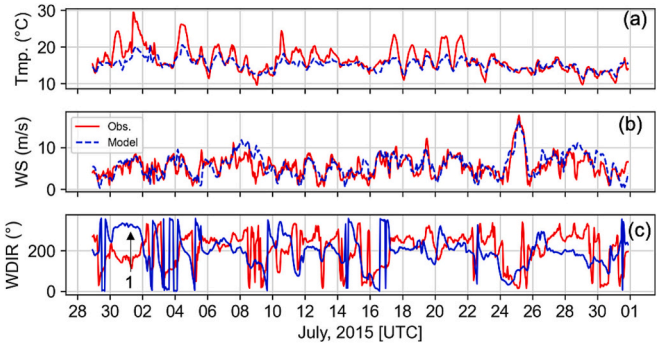

Fig. 3. Measured and modelled meteorological variables: a) temperature (°C), b) wind speed (m/s), and c) wind direction (°), at WAO, from June 29th to July 31st 2015. Number 1 in the plot highlight the difficulty of the model capturing the south easterly winds. The study episode is highlighted in gey.

from NO, NO_2, Nitrate Radical (NO_3), peroxynitric acid (HO_2NO_2), dinitrogen pentoxide (N_2O_5), peroxyacetyl Nitrate (PAN), peroxynitrate (ONIT), methacryloyl peroxynitrate (MPAN), isoprene nitrates ($ISOPNO_3$), and organic nitrates (ONITR). The model captures much of the observed day-to-day variability for NO_x, NO_y, CO, and O_3, with correlation coefficients of 0.60, 0.65, 0.67, and 0.78, respectively. However, NO_y shows a notable negative bias of −2 ppbv (see Figs. S.2.1d and S.2.2d), potentially due to challenges in the MOZART chemical mechanism's handling of NO_y recycling and the long-range transport of NO_y. In addition, a large negative mean bias is observed in NO_2 (−0.39 ppbv) and NO_x (0.43 ppbv), which can be attributed to biases in ingested emissions and/or challenges in accurately representing NO_2 production. Fig. 2 shows that on July 1st, the day with the highest observed O_3 mixing ratios, modelled NO_2 overestimates observations at night (MB = 0.41 ppbv) and significantly underestimates values during the day (MB = −2.5 ppbv). For the remainder of the campaign (blue line), modelled mean mixing ratios are closer to observations but remain underestimated (dashed line), with a daytime MB of −0.36 ppbv and a night-time MB of −0.51 ppbv.

The difficulty of chemical transport models in capturing observed NO and NO_2 concentrations, particularly their tendency to underestimate NO_2 during the day and overestimate it at night, especially in summer, has been well documented (e.g., Kuhn et al., 2024; Pirovano et al., 2012; Tuccella et al., 2012). This issue has been repeatedly observed across different regions, spatial resolutions, emission datasets, boundary layer parameterizations, and chemical mechanisms. Even at finer horizontal resolutions, such as the 5 km simulations in Lupaşcu et al. (2022), these biases persist. Kuhn et al. (2024) attributed this persistence bias to faulty diurnal emission profiles and/or insufficient vertical mixing at night. Adjusting the vertical mixing parameterization in different boundary layer schemes has been shown to significantly reduce the bias. Specifically, increasing the lower mixing threshold enhances vertical mixing at night, mainly affecting the surface layer, which in turn reduces night-time NO_2 overestimation (Kuhn et al., 2024).

Our results align with findings from background sites in source attribution studies over Germany at a 5 km resolution (Lupaşcu et al., 2022). Improving the representation of NO_2 in the model requires further investigation into the impact of different NO/NO_2 emission partitioning approaches and variations in diurnal emission distributions. Additionally, incorporating vertical emission profiles could enhance model performance, particularly over the UK, where high-resolution emission data (1 km × 1 km) are available. However, increasing the model resolution accordingly would necessitate a reduction in the geographical coverage of the model domains, which falls beyond the scope of this study.

Conversely, the model does a good job of capturing the diurnal cycle of most assessed species, as shown in Fig. S.2.2. NO mixing ratios are

underestimated at night, with modelled NO often reaching zero, whereas observed values can reach up to 0.3 ppbv (see Fig. S.2.2a in the suplemental material). CO mixing ratios tend to be overestimated, especially during periods with westerly winds (e.g., on June 29 and from July 5–8), as shown in Fig. S.2.1e.

The model overestimates wind speeds when the prevailing wind direction is south-westerly (SW) (see Fig. 4). In western UK regions, westerly winds generally bring clean air masses from the Atlantic, so the model's SW bias may relate to the dispersion of some species, potentially reducing CO mixing ratios near background levels. However, in the eastern UK, especially at WAO, this bias likely highlights the influence of transported polluted air from nearby urban centres such as London and Birmingham. Despite these issues, hourly CO concentration variations are well represented, with a slight positive bias (MB = 11 ppbv). O_3 mixing ratios are also well modelled, showing a small negative bias (MB = −2 ppbv).

The model struggles to capture peak O_3 levels on July 1st, when observed mixing ratios exceeded 90 ppbv, as shown in Fig. 2 and in Figs. S.2.1f and S.2.2f in the supplemental material. Romero-Alvarez et al. (2022) highlight that the current model configuration significantly underestimated isoprene mixing ratios, particularly during the early days of July. Elevated temperature-driven isoprene mixing ratios have been widely reported during peak O_3 events in Southeast UK (e.g., Lee et al., 2006), emphasizing the role of isoprene as a key precursor in the formation of O_3 under high-temperature conditions. This underestimation likely contributed to the model's difficulty in capturing the observed O_3 peaks. Furthermore, while the evaluation presented focuses on very local wind directions, challenges in accurately simulating wind fields may have also affected the model's ability to represent O_3 levels during the peak day. In the model, the highest O_3 values are associated with south-easterly winds, whereas observational data suggest that maximum values occurred under more southerly winds. A similar pattern is evident for CO (Fig. 4b), indicating that the model may not fully capture the impact of wind speed and direction shifts on O_3 and CO levels. In contrast, no clear trends are observed for NO and NO_2. In the East of England, wind direction plays a crucial role during high O_3 episodes, often driven by the transport of O_3 and its precursors from continental Europe under anticyclonic conditions (AQEG, 2009). Future trajectory analyses could provide further insights into these discrepancies by elucidating the transport pathways that influence local O_3 levels. Despite these challenges, Fig. 5 demonstrates that the model successfully captures the geographical extent and evolution of the pollution episode, showing high values across western Europe and eastern England. Therefore, we investigate the impact of NO_x emissions from different tagged regions on the observed low bias in O_3 mixing ratios.

3.3. Ozone contributions from different geographical source regions

Fig. 6 presents the absolute contributions of O_3 sources from lateral boundaries (LBC), North Sea and English Channel (NOS), domestic emissions (UK), and European regions, to surface O_3 levels at four sites across the East of England from June 30th to July 4th, 2015. Table 2 summarizes the maximum contributions to surface O_3 at the four sites for each day.

Similar to Lupaşcu et al. (2022), the meteorology played a key role in the relative influence of local vs. transboundary O_3 sources. Overall, lateral boundary contributions (LBC, dark purple) were substantial across all sites, peaking on July 2nd at 32.5 ppbv (66.0 %) at WAO and 35.6 ppbv (70.0 %) at Sibton. Beyond LBC, contributions from BENELUX (greenish-blue), Germany (bright green), France (greenish-yellow), NOS

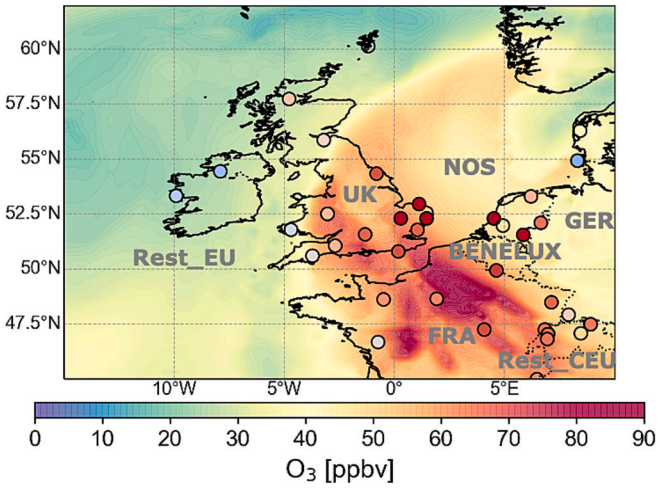

Fig. 5. Overlaid average of surface O_3 in the afternoon (12:00 to 18:00 UTC) on the 1st of July 2015 in the UK and Western Europe for model (contours) and observations from EMEP stations with altitude <400 m (coloured circles). Tagged regions are included as a reference.

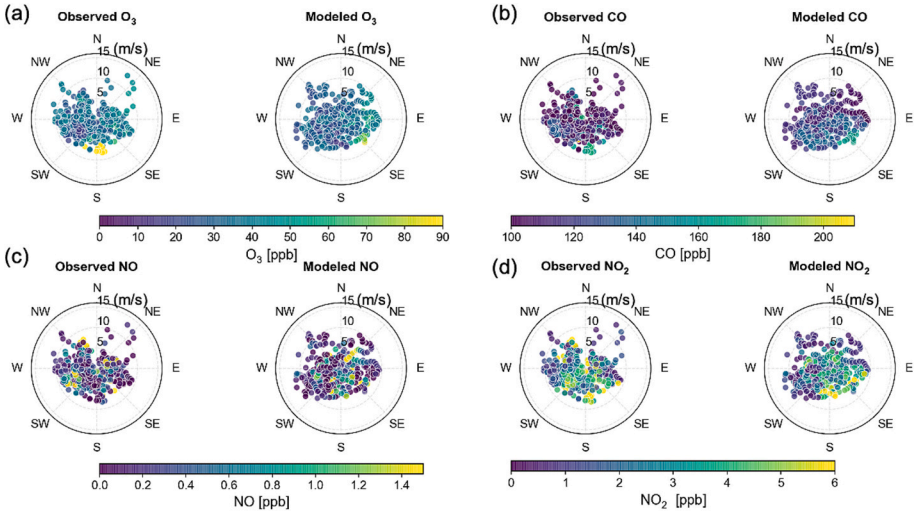

Fig. 4. Pollution roses comparing observed (left subpanel) with modelled (right subpanel) data for O_3 (a), CO (b), NO (c) and NO_2 (d) at WAO using data from June 29th to July 31st 2015. The distribution and spread of data points around the circle indicate which wind directions are associated with higher or lower pollutant levels. The radians represent the wind speed in m/s.

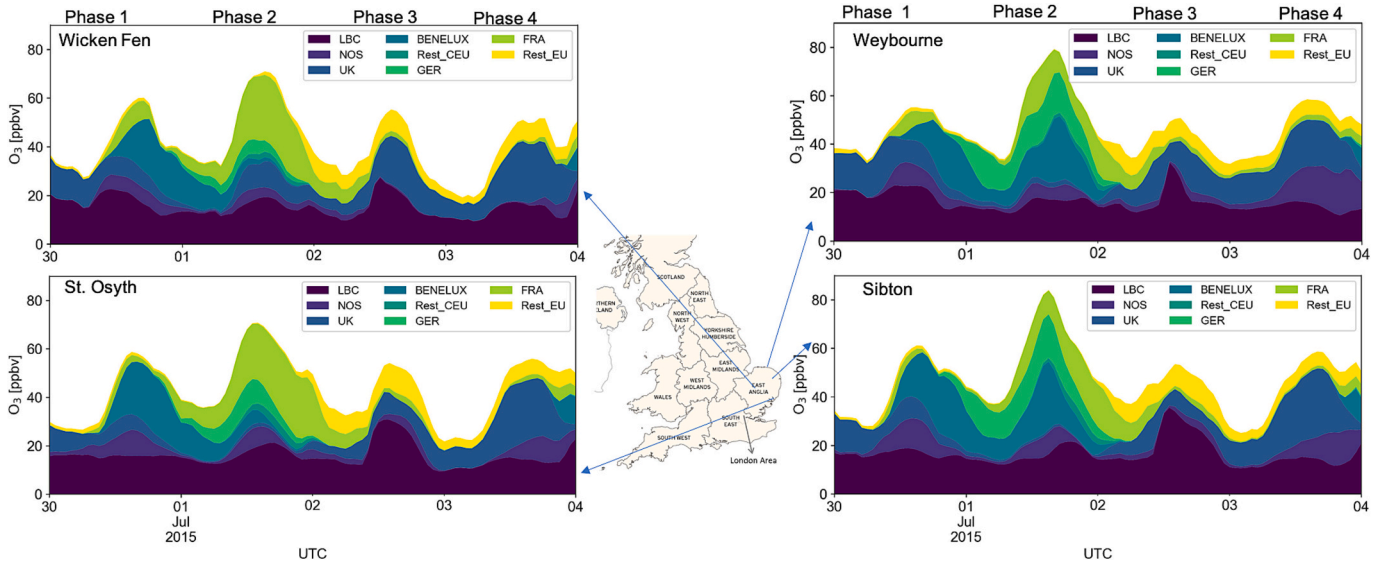

Fig. 6. Contributions to hourly near surface O_3 at four sites in the East of England from June 30th to July 4th 2015. Phase 1 to 4 refers as the different stages of the episode.

Table 2
Maximum daily contributions (ppbv and percentage) from eight source regions to surface O_3 over Weybourne (blue), Sibton (orange), St. Osyth (grey) and Wicken Fen (yellow). The maximum contributions during the peak O_3 event are highlighted in red. The reported values correspond to the contributions from anthropogenic sources only.

Source region	LBC	NOS	UK	BENELUX	Rest_CEU	GER	FRA	Rest_EU
June 30th	24.0 (18.5 %)	10.0 (18.5 %)	19.1 (44.8 %)	21.3 (46.6 %)	0.0 (0.0 %)	3.6 (8.2 %)	7.5 (14.1 %)	2.0 (5.4 %)
July 1st	18.0 (25.5 %)	6.9 (9.5 %)	2.7 (6.4 %)	26.7 (34.1 %)	2.9 (5.6 %)	17.4 (22.0 %)	17.0 (24 %)	0.7 (1.6 %)
July 2nd	32.5 (66.0 %)	3.9 (8.7 (%)	17.5 (38.5 %)	4.7 (11.0 %)	2.5 (5.7 %)	4.3 (10.0 %)	14.1 (34.0 %)	8.2 (20.4 %)
July 3rd	16.3 (29.2 %)	18.3 (35.8 %)	19.3 (33.0 %)	6.4 (23.9 %)	0.1 (0.2 %)	0.7 (1.5 %)	3.6 (7.2 %)	6.3 (10.9 %)
July 4th	13.4 (27.9 %)	10.9 (22.7 %)	5.4 (11.3 %)	8.6 (17.8 %)	0.1 (0.3 %)	1.0 (2.0 %)	3.7 (7.8 %)	4.8 (10.0 %)
June 30th	18.9 (32.5 %)	12.8 (20.8 %)	14.8 (43.0 %)	24.5 (47.3 %)	0.0 (0.0 %)	6.0 (12.6 %)	5.1 (11.0 %)	2.1 (5.3 %)
July 1st	21.7 (34.0 %)	9.0 (10.7 %)	2.0 (4.4 %)	28.4 (34.5 %)	4.2 (6.8 %)	18.1 (22.7 %)	17.7 (30.7 %)	0.8 (1.7 %)
July 2nd	35.6 (70.0 %)	3.7 (8.4 %)	13.1 (29.0 %)	4.1 (8.8 %)	2.5 (5.3 %)	4.7 (10.0 %)	17.5 (38.6 %)	10.0 (20. 8 %)
July 3rd	17.2 (31.7 %)	13.7 (26.2 %)	28.2 (48.0 %)	12.5 (23.0 %)	0.1 (0.2 %)	0.6 (1.1 %)	4.8 (9.0 %)	6.0 (11.8 %)
July 4th	21.2 (42.0 %)	5.4 (10.6 %)	2.5 (5.0 %)	10.4 (20.6 %)	0.2 (0.4 %)	0.8 (1.5 %)	4.6 (9.2 %)	5.3 (10.6 %)
June 30th	16.5 (60.6 %)	10.9 (18.5 %)	11.1 (37.0 %)	24.1 (43.9 %)	0.0 (0.0 %)	1.8 (4.1 %)	6.6 (15.4 %)	2.0 (6.9 %)
July 1st	21.3 (32.2 %)	8.2 (11.6 %)	2.6 (5.0 %)	12.7 (33.0 %)	3.7 (5.8 %)	11.0 (16.1 %)	27.6 (47.2 %)	3.2 (6.2 %)
July 2nd	30.9 (58.1 %)	4.6 (9.3 %)	11.4 (34.2 %)	0.4 (0.8 %)	0.8 (1.7 %)	0.9 (1.7 %)	21.0 (42.5 %)	11.1 (21.2 %)
July 3rd	20.5 (39.3 %)	11.0 (20.1 %)	26.0 (50.0 %)	12.0 (23.2 %)	0.1 (0.2 %)	0.2 (0.4 %)	5.5 (10.9 %)	6.6 (12.6 %)
July 4th	23.0 (46.0 %)	3.8 (7.6 %)	2.1 (4.3 %)	11.2 (22.4 %)	0.2 (0.3 %)	0.3 (0.6 %)	3.8 (7.6 %)	5.4 (10.9 %)
June 30th	22.7 (52.1 %)	6.4 (10.7 %)	15.2 (41.3 %)	23.3 (40.2 %)	0.0 (0.0 %)	1.4 (3.5 %)	8.5 (14.5 %)	2.1 (4.8 %)
July 1st	19.4 (27.2 %)	5.2 (7.7 %)	11.0 (15.7 %)	14.8 (39.0 %)	2.2 (3.2 %)	6.0 8.7 %)	27.8 (40.6 %)	6.4 (15.3 %)
July 2nd	27.5 (54.5 %)	2.7 (8.3 %)	20.6 (39.4 %)	0.05 (0.1 %)	0.1 (0.2 %)	0.1 (0.2 %)	6.9 (18.5 %)	8.9 (16.2 %)
July 3rd	17.3 (36.5 %)	6.8 (16.9 %)	25.0 (48.9 %)	6.1 (12.7 %)	0.1 (0.2 %)	0.1 (0.2 %)	4.9 (10.1 %)	8.0 (15.6 %)
July 4th	23.0 (45.3 %)	4.4 (8.6 %)	2.8 (5.4 %)	9.9 (19.4 %)	0.1 (0.2 %)	0.2 (0.3 %)	4.6 (9.0 %)	5.9 (11.5 %)

(light purple), and Rest_EU (yellow) varied by site and atmospheric conditions.

On June 30th, phase one of the episode, easterly and south-easterly winds drove significant O_3 contributions from local and transboundary sources. BENELUX dominated transboundary inputs, peaking at 46.6 % (21.3 ppbv) at Weybourne and 47.3 % (24.5 ppbv) at Sibton. UK sources were substantial inland, contributing up to 41.3 % (15.2 ppbv) at Wicken Fen and 43.0 % (14.8 ppbv) at Sibton. LBC influence was highest at Wicken Fen (52.1 %) and St. Osyth (60.6 %), while NOS impacted coastal sites, reaching up to 18.5 % (10.0 ppbv) at Weybourne. GER and FRA had smaller contributions, with GER peaking at 12.6 % (6.0 ppbv) at Sibton and FRA at 14.5 % (8.5 ppbv) at Wicken Fen.

On July 1st, south-easterly winds strengthened, driving the highest observed O_3 levels across the East of England. Approximately 60 % of the daily mean surface O_3 originated from non-UK sources across the study region, with 30 % from lateral boundaries (LBC) and only ~4 % from UK emissions, as shown in Fig. S.3.1. in the supplemental material. The prevailing winds transported substantial O_3 and precursors from Western Europe, with BENELUX (up to 26.7 ppbv, 34.1 %), Germany (up to 17.4 ppbv, 22.0 %), and France (up to 17.0 ppbv, 22.0 %) contributing significantly at Weybourne. At Sibton, transboundary inputs were dominated by BENELUX (up to 28.4 ppbv, 34.5 %), Germany (up to 18.1 ppbv, 22.7 %), and France (up to 17.7 ppbv, 30.7 %).

This peak episode coincided with a convergence ($-0.00002\ s-1$) of strong south-easterly winds and weaker westerlies in the west of the UK, redistributing domestic O_3 northward and westward, as illustrated by Figs. 7 and S.3.2 in the supplement, while amplifying continental influences across all sites. At Wicken Fen, BENELUX contributed up to 14.8 ppbv (39.0 %) and France up to 27.8 ppbv (40.6 %), while UK sources remained modest up at to 11.0 ppbv (15.7 %). The transport patterns observed align with high-O_3 episodes in the UK, where high-pressure systems over northwest Europe sustain easterly and south-easterly flows that enhance O_3 accumulation and long-range transport (Jenkin et al., 2002; Pope et al., 2016). The dominance of BENELUX, Germany, and France in transboundary pollution highlights the importance of regional collaboration in mitigating episodic O_3 pollution, as similar

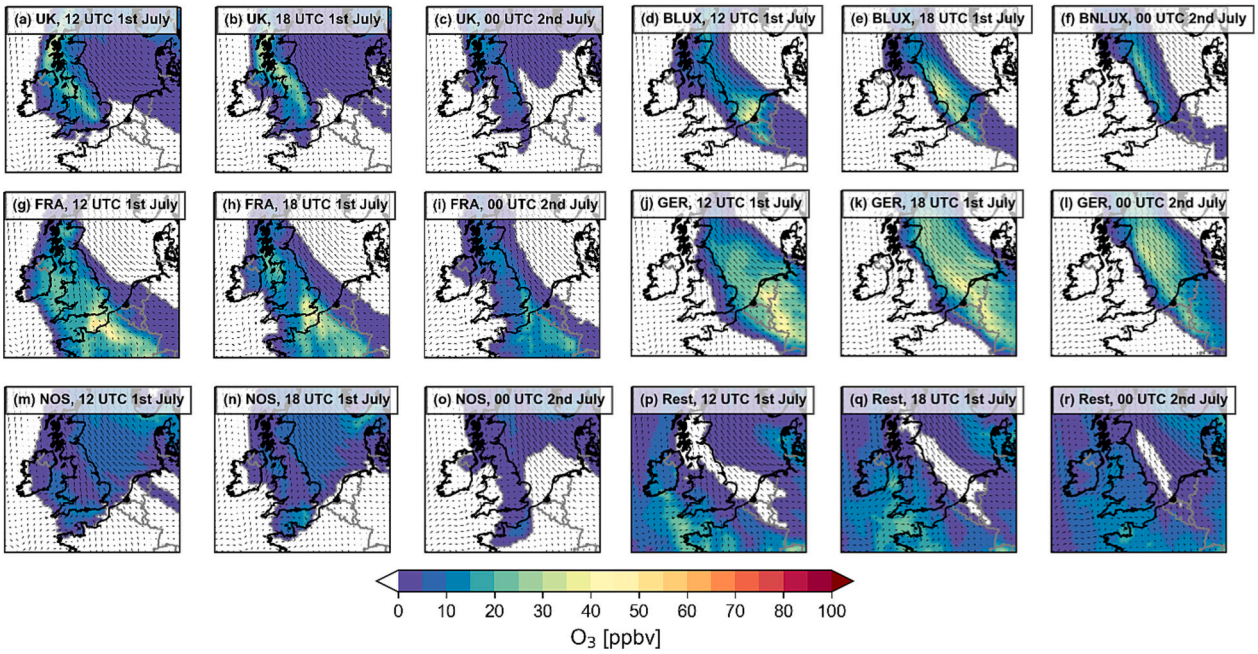

Fig. 7. Modelled O_3 mixing ratios contributions to total O_3 from the UK, BENELUX (BNLUX), FRA, GER, NOS and the rest of the source regions (Rest) and winds on July 1st 12:00 (a, d, g, j, m, p), 18:00 (b, e, h, k, n, q) and 2nd of July at 00 UTC (c, f, i, l, o, r). Black arrows depict 10 m winds. The red arrows indicate the convergence of westerly and easterly winds.

circulation patterns have been associated with exceedances of the 90th percentile of of O₃ levels in these regions during spring and summer (Ordóñez et al., 2017; Otero et al., 2022).

On July 2nd, a shift to south-south-westerly winds increased the influence of local sources, with domestic NO_x emissions contributing over 35 % to surface O₃. At Wicken Fen, UK emissions reached 20.6 ppbv (39.4 %), while at Sibton, they accounted for 13.1 ppbv (29.0 %), contrasting with the earlier phase dominated by transboundary sources. France and Rest_EU remained significant contributors, particularly at St. Osyth, where France provided up to 21.0 ppbv (42.5 %) and Rest_EU 11.1 ppbv (21.2 %). At Weybourne, France contributed 14.1 ppbv (34.0 %) and Rest_EU 8.2 ppbv (20.4 %), indicating continued long-range transport, likely from the Iberian Peninsula and Atlantic shipping routes. NOS contributions were moderate, peaking at 4.6 ppbv (9.3 %) at St. Osyth and 3.9 ppbv (8.7 %) at Weybourne. The influence of BENELUX and Germany declined compared to previous days, with BENELUX contributing up to 4.7 ppbv (11.0 %) at WAO, while Germany peaked at 4.7 ppbv (10.0 %) at Sibton.

On July 3rd, a shift to predominantly easterly winds elevated the influence of domestic sources (UK) and NOS, making them the primary contributors to surface O₃ across the East of England. UK emissions were the dominating source, contributing up to 48.9 % of O₃ at Wicken Fen and 50.0 % at St. Osyth, while NOS contributions were substantial, peaking at 35.8 % at Weybourne and 26.2 % at Sibton, highlighting the influence of nearby coastal emissions. Although Western European sources (France and BENELUX) were minimal during the day, their influence increased in the evening, with BENELUX reaching 12.7 % and France 10.1 % at Wicken Fen. At St. Osyth, France contributed 10.9 %, while Rest_EU peaked at 15.6 % at Wicken Fen, likely driven by long-range transport from south-eastern Europe and Atlantic shipping routes. Long-range transport from Rest_EU and Western Europe continued as a secondary but significant factor, particularly in the evening.

3.4. Factors leading to the ozone build-up

Fig. 8 presents curtain plots for four sites in the East of England, illustrating the modelled rate of change in O₃ mixing ratios driven by advection, vertical mixing, and net chemical production. Supplementary Figs. S.3.3–S.3.7 further detail the contributions from various source regions. These tagged O₃ tendencies provide insights into the total O₃ evolution but are subject to biases arising from the model's coarse resolution, the documented negative O₃ bias, and the exclusion of VOCs in the tagging scheme. Additionally, Fig. S.3.8 in the supplementary material report the estimated O₃ flux (ppb h^{-1}) just above the boundary layer top.

Across the region, the O₃ rate of change exhibited significant diurnal and spatial variability, driven by photochemistry, advection, and vertical mixing. Chemical processes were the primary driver of the daily increase in O₃, contributing an average of 42 ppbv per day during the peak O₃ day. In contrast, vertical mixing played a dominant role at St. Osyth, contributing up to 74 ppbv and 16 ppbv to the total O₃ on June 30th and July 1st, respectively, as illustrated in Fig. S.3.9 in the supplementary material. On June 30th, during phase one of the episode, most sites experienced a marked increase in near-surface O₃ mixing ratios during the early morning (Fig. 8, panels a and b). Positive O₃ vertical mixing tendencies near the surface, combined with negative values at the top of the PBL between 400 and 800 m (at Wicken Fen, St. Osyth, and Sibton, indicated by numbers 1, 2, and 3 respectively in Fig. 8), suggest efficient boundary layer mixing, transporting ozone-rich air from the residual layer to the surface. Fig. S.3.8 further illustrates that O₃ entrainment flux at the boundary layer top can reach up to 9 ppb h^{-1} in the morning at Wicken Fen and 8 ppb h^{-1} at WAO. Note that the changes in the O₃ flux are driven by boundary layer growth; however, their magnitude can also be influenced by advection, deposition, and chemical production/loss.

Concurrently, chemical loss near the surface was also observed at St. Osyth and Sibton, as indicated by numbers 4 and 5 in Fig. 8. Time-series tendencies in Fig. 9 highlight the critical role of vertical mixing, contributing up to 35.7 % of the total modelled O₃ mixing ratio at St. Osyth at 10:00 am. Advection showed moderate consistency across sites, accounting for 1–12 % of total O₃ mixing ratios. Around midday (09:00–15:00 UTC), photochemical production emerged as a dominant process, driving the positive increase in the near-surface O₃ mixing

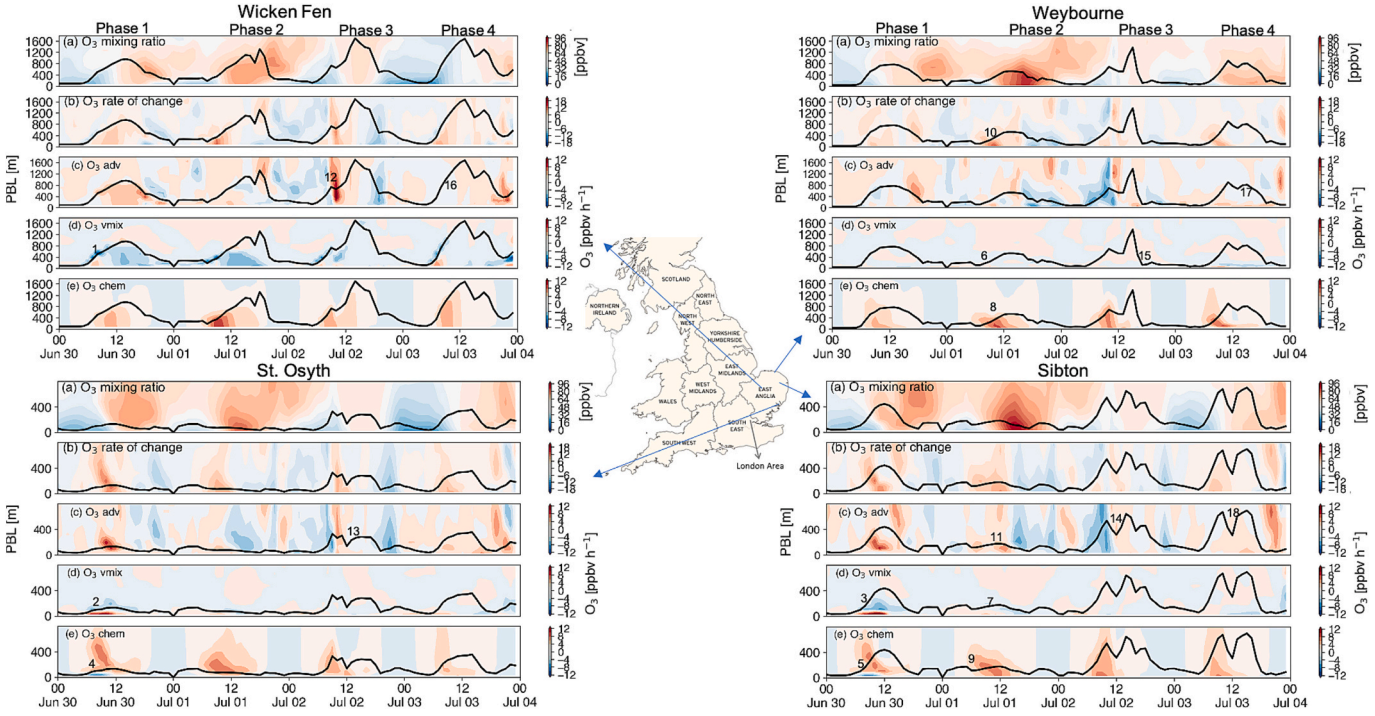

Fig. 8. Curtain plots of modelled O_3 mixing ratios (ppbv) and process tendencies (ppbv h^{-1}) from June 30th to July 4th 2015.UTC, at four sites in the East of England. Panel (a) depicts the total O_3 mixing ratios, (b) the rate of change in O_3 (c) contribution from advection, (d) the vertical mixing, and (e) O_3 chemical tendency. The black line shows the evolution of the PBL. The numbers in the panels (1–18) correspond to changes in the tendencies discussed in the text.

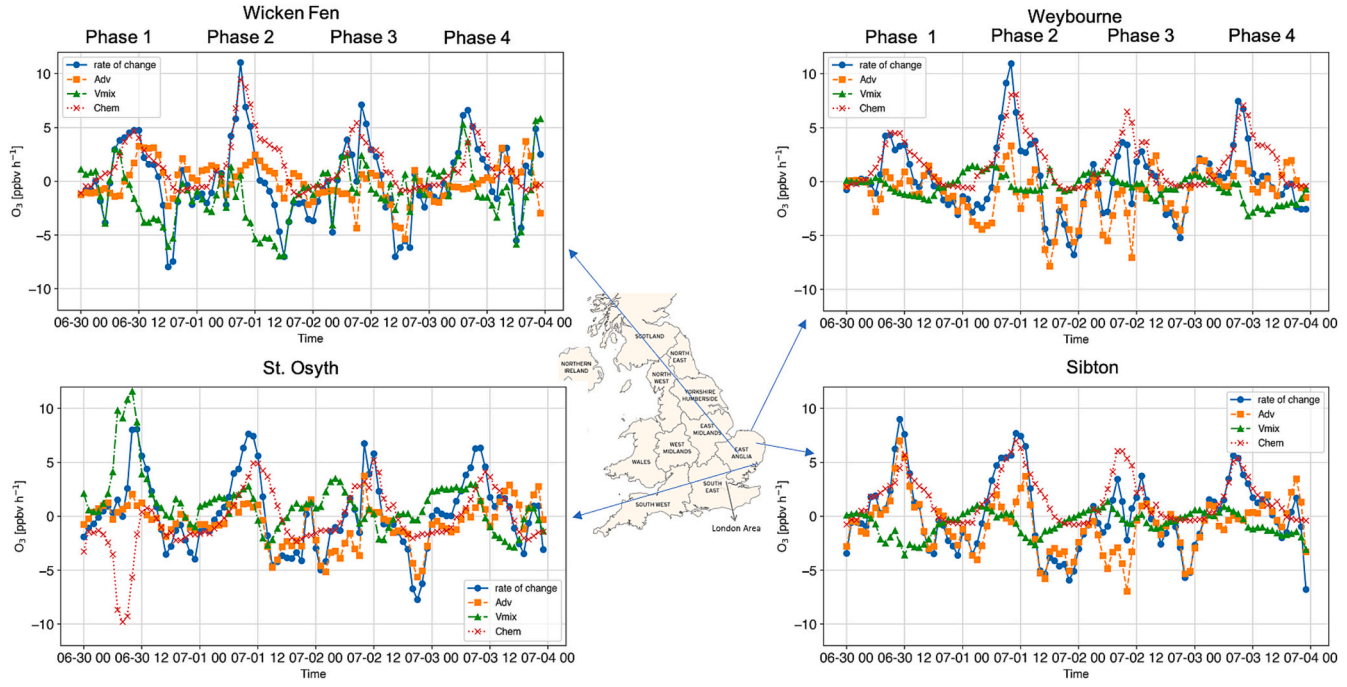

Fig. 9. Time series of near-surface modelled O_3 rate of change (ppbv h^{-1}) and process tendencies from June 30th to July 4th 2015 UTC, at four sites in the East of England.

ratios. Fig. 9 shows sharp midday peaks at most sites, suggesting that local processes can play a more prominent role during specific episodes. In contrast, regional transport tends to dominate when O_3 levels are assessed over broader spatial and temporal scales. as shown in Romero-Alvarez et al. (2022). These peaks were primarily driven by NO_x emissions from domestic sources and the NOS region, as evidenced by the curtain plots of modelled O_3 mixing ratios and process tendencies (Figs. S.3.4 and S.6), and by the time series of near-surface O_3 rate of change and process tendencies (Figs. S.3.11 and S.3.13). Advection remained an important process, particularly at Wicken Fen and Sibton, contributing up to 6 % of the total modelled O_3 mixing ratio. Afternoon hours saw a loss in the O_3 mixing ratios driven by deposition and

chemical reaction with NO_x.

On the 1st of July, O_3 mixing ratios peaked across all sites due to a synergy of vertical mixing, photochemical production and advection of ozone-rich air mases. The early morning was dominated by contributions from vertical mixing across most sites, persisting until noon (Fig. 9). As the PBL developed throughout the morning, ozone-laden air was effectively mixed into the surface layer (at WAO and Sibton, indicated by numbers 6 and 7 respectively in Fig. 8). At the boundary layer top, O_3 entrainment flux reached up to 10 ppb h^{-1} at WAO, as shown in Fig. S.3.8 in the supplemental material. Concurrently, photochemical production began after 6 am, further driving the increase in O_3 mixing ratios (at WAO and Sibton as indicated by numbers 8, 9, 10 and 11 in Fig. 8). Analysis of PAN at WAO revealed a reservoir above the PBL, which became available for downward mixing in the early morning. This indicates an inflow of chemically processed air over WAO. Surface-level PAN mixing ratios reached up to 1.20 ppbv between 08:00 UTC and just before midday (Fig. 10a). Furthermore, Fig. 10b-f highlights significant contributions from multiple regions, including NOS, GER, BENELUX, FRA, and the UK. As a product of NO_x photochemistry, PAN plays a crucial role in transporting O_3 precursors to less polluted areas (HTAP, 2007). Its stability under cold conditions allows for long-range transport within the free troposphere. When PAN descends to surface levels, it thermally decomposes, producing a peroxyacetyl radical (PA) and NO_2 (Fischer et al., 2014). The PA radical can either reform PAN by reacting with NO_2 or react with NO to generate additional NO_2.

The highest rate of change in near-surface O_3 mixing ratios was predicted around midday, between 11 and 13 UTC, with photochemical production peaking across all sites and contributing, on average, about 7 % of the total modelled O_3 mixing ratio. NO_x emissions from FRA, BENELUX, NOS, and Germany played a key role in local O_3 formation, with the NOS region contributing up to 5 %, 3 %, 5 %, and 7 % to the total modelled O_3 mixing ratio at St. Osyth, WAO, Wicken Fen, and Sibton, respectively (see the chemical tendency represented by the red line in Figs. S.3.10, S.3.12, S.3.13, and S.3.14, respectively). Local emissions, on the other hand, played a significant role at Wicken Fen and Weybourne, contributing approximately 4 % and 2 % to the total modelled O_3 mixing ratios, respectively, as shown in Fig. S.3.11 in the supplemental material emphasizing the importance of nearby anthropogenic sources. Similar features were observed during the 2003 UK heatwave, where Lee et al. (2006) highlighted the critical role of regional transport and vertical mixing in incorporating ozone-laden air into the surface layer during morning hours, followed by intensified photochemical production in the afternoon under anticyclonic conditions.

Afternoon hours saw advection weaken across most sites, with chemical O_3 production and vertical mixing becoming the dominant processes. Fig. 8 illustrates diminishing O_3 fluxes at higher altitudes (~800–1200 m), consistent with a reduced role of regional transport. At night, curtain plots in Fig. 8 show limited O_3 transport, with mixing ratios stabilizing below 1000 m. FRA, UK, and NOS contributions remained reduced but consistent, varying by site, as depicted in Fig. S.3.10, S.3.11, and S.3.13 in the supplemental material.

On July 2nd, during phase three of the episode, O_3 mixing ratios declined slightly, showing a shift toward more localized contributions. Domestic sources and NOS played significant roles in O_3 build-up at most sites. Curtain plots in Fig. 8 illustrate sustained near-surface advection of ozone-rich air at Wicken Fen, St. Osyth, and Sibton, indicated by numbers 12, 13, and 14, respectively. Evidence of O_3 depletion due to horizontal outflow is also observed, particularly at surface levels (indicated by number 15 in Fig. 8). This is further supported by Figs. S.3.10 to S.3.14 in the supplemental material, which highlights sustained outflows of ozone-rich air from tagged regions such as FRA, BENELUX, and GER.

Morning hours exhibited dynamics similar to those on July 1st, with vertical mixing facilitating the downward transport of ozone-laden air from the residual layer, followed by chemical production and advection, as shown in Fig. 9. At most sites, O_3 entrainment fluxes at the boundary layer top exceeded 6 ppb h^{-1}, as shown in Fig. S.3.8 in the suplemental material. By midday, moderate O_3 peaks were recorded across all sites, with photochemical production becoming the dominant contributor, accounting for about 10 % of the total O_3 mixing ratios. This increase was driven primarily by domestic NO_x emissions, as detailed in Figs. S.3.4 and S.3.11 in the supplemental material. At sites such as Wicken Fen, local NO_x emissions contributed up to 9 % of in situ chemical formation to the total O_3 mixing ratios. Advection contributions further decreased in the afternoon hours, however small contributions from France, domestic UK, and NOS sources remained evident. Vertical mixing continued to dominate at St. Osyth, contrasting with the advection-driven patterns observed at other sites.

By July 3rd, the final phase of the episode, O_3 levels decreased further as regional transport contributions weakened. During the morning hours, advection from foreign sources diminished, while domestic and NOS advection of ozone-rich air masses played a key role in surface O_3 build-up. Curtain plots in Fig. 8 (at Wicken Fen, Weybourne and Sibton indicated by numbers 16, 17, and 18 respectively) illustrate this reduction in O_3 inflow, reflecting the overall decline in regional contributions, as further supported by time series data in Figs. S.3.10 and S.3.13 in the supplemental material. By midday, photochemical production emerged as the dominant process, contributing up to 10 % of the total O_3 mixing ratios across all sites, as surface O_3 build-up shifted to more localized sources, as shown in Fig. 9. In the afternoon, vertical mixing at St. Osyth played a critical role in redistributing O_3 throughout

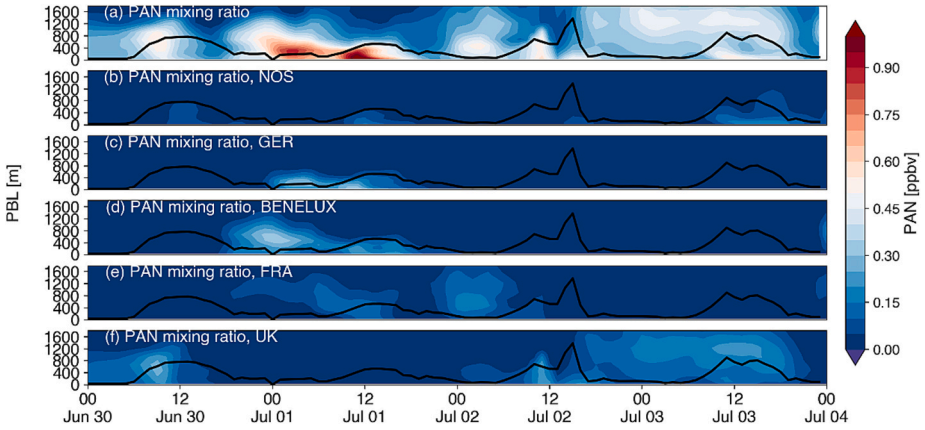

Fig. 10. Curtain plots of PAN mixing ratios (ppbv) from June 30th to July 4th 2015, at Weybourne for (a) total mixing ratios, and contributions from (b) NOS, (c) GER, (d) BENELUX, (e) FRA, and (f) UK.

the PBL. Although weakened, advection remained active across all sites, sustaining surface mixing ratios with contributions from FRA, BENELUX, and NOS. These patterns underscore a shift toward localized photochemical production as the primary driver of O_3 dynamics on the final day of the episode.

4. Conclusions

Ozone-tagging has been employed to quantify the contributions of domestic and overseas NO_x emissions to surface ozone build-up in East England during the July 2015 high-pollution episode, which was characterized by a widespread high-pressure system that brought elevated temperatures and high O_3 mixing ratios in the evening.

Numerical simulations have shown that on the day O_3 mixing ratios peaked, south-easterly winds carried significant O_3 and its precursors from mainland Europe, with BENELUX, France, Germany, the North Sea and the English Channel together accounting for approximately 60 % of daily mean O_3. The contribution from these transboundary sources significantly exceeded that of domestic UK emissions (~4.6 %), emphasizing the importance of regional transport during favourable meteorological conditions. Convergence ($-0.00002\ s^{-1}$) of strong south-easterly winds and weaker westerlies in the west of the UK, redistributing domestic O_3 northward and westward, while amplifying continental influences across the study region.

As the episode progressed, easterly winds increased the impact of local sources, especially from domestic emissions and maritime activities in the North Sea and English Channel.

This analysis has also highlighted key mechanisms contributing to the O_3 build-up. In the mornings, vertical mixing facilitated the transport of ozone-rich air downwards from the residual layer, increasing surface O_3 mixing ratios by up to 16 ppbv on the peak O_3 day. By midday, local photochemical production driven by both domestic and transported NO_x emissions dominated, contributing up to 42 ppbv per day. These findings reinforce earlier studies, such as Lee et al. (2006), underscoring the combined roles of regional transport, vertical mixing in the morning, and intensified afternoon photochemistry under anticyclonic conditions. Additionally, the availability of chemical reservoirs like peroxyacetyl nitrate (PAN) illustrates how transported precursors sustain local O_3 production.

Our findings underline the importance of coordinated international efforts to manage transboundary pollution, especially from industrialized regions of EU and maritime sources around the North Sea and English Channel. Effective air quality management must integrate regional cooperation with targeted local measures, particularly during heatwave conditions.

CRediT authorship contribution statement

Johana Romero-Alvarez: Writing – original draft. **Aurelia Lupaşcu:** Writing – review & editing, Software, Methodology. **Steve Dorling:** Writing – review & editing, Supervision, Resources, Methodology, Investigation. **Claire E. Reeves:** Writing – review & editing, Supervision, Methodology, Investigation, Funding acquisition. **Tim Butler:** Software, Methodology, Funding acquisition.

Financial support

This research has been supported by the European Research Council, FP7 Ideas (ASIBIA (grant no. 616938)); the University of East Anglia, UK; the Federal Ministry of Education and Research of Germany (BMBF); and the Ministry for Science, Research and Culture of the state of Brandenburg (MWFK; grant no. 01US1701).

Declaration of competing interest

We declare no competing financial interest.

Acknowledgements

The authors would like to thank Dr. Fabio Di Gioacchino for reviewing the document for language clarity and formatting. We also thank TNO for access to the TNO-MACC-III emissions inventory. The WRF-Chem simulations were performed on the high-performance research computer of the University of East Anglia, UK. We acknowledge the use of the WRF-Chem pre-processor tools (bio_emiss and fire_emiss, mozbc) provided by the Atmospheric Chemistry Observations & Modelling Lab (ACOM) of NCAR. This research was supported in part by the NOAA cooperative agreement NA22OAR4320151, for the Cooperative Institute for Earth System Research and Data Science (CIESRDS). The statements, findings, conclusions, and recommendations are those of the author(s) and do not necessarily reflect the views of NOAA or the U.S. Department of Commerce.

Appendix A. Supplementary data

Supplementary data to this article can be found online at https://doi.org/10.1016/j.scitotenv.2025.179464.

Data availability

The WRF-Chem model is publicly available at https://www2.mmm.ucar.edu/wrf/users/download/get_source.html (last accessed: 16 December 2024). The modification of the code, model output and script for the analysis are available online via Zenodo at https://zenodo.org/records/6968649, doi:https://doi.org/10.5281/zenodo.6968649 and https://zenodo.org/records/14956680.

References

AQEG, 2009. Ozone in the United Kingdom.

Archer-Nicholls, S., Lowe, D., Utembe, S., Allan, J., Zaveri, R.A., Fast, J.D., Hodnebrog, Ø., 2014. Gaseous chemistry and aerosol mechanism developments for version 3.5.1 of the online regional model. WRF-Chem. Geoscientific Model Development 7, 2557–2579. https://doi.org/10.5194/gmd-7-2557-2014.

Atkinson, R., 2000. Atmospheric chemistry of VOCs and NOx. Atmos. Environ. 34 (12–14), 2063–2101. https://doi.org/10.1016/S1352-2310(99)00460-4.

Butler, T., Lupaşcu, A., Coates, J., Zhu, S., 2018. TOAST 1.0: Tropospheric ozone attribution of sources with tagging for CESM 1.2.2. Geosci. Model Dev. 11 (7), 2825–2840. https://doi.org/10.5194/gmd-11-2825-2018.

Butler, T., Lupaşcu, A., Nalam, A., 2020a. Attribution of ground-level ozone to anthropogenic and natural sources of nitrogen oxides and reactive carbon in a global chemical transport model. Atmos. Chem. Phys. 20 (17), 10707–10731. https://doi.org/10.5194/acp-20-10707-2020.

Butler, T., Lupaşcu, A., Nalam, A., 2020b. Attribution of ground-level ozone to anthropogenic and natural sources of nitrogen oxides and reactive carbon in a global chemical transport model. Atmos. Chem. Phys. 20 (10707–10731), 1–41. https://doi.org/10.5194/acp-2020-436.

CAMS. (2016). *Interim annual assessment report for 2015 - European air quality in 2015 interim annual assessment report* (issue September). Doi:10.13140/RG.2.2.15127.78249.

Crilley, L., Kramer, L., Reed, C., Lee, J.D., Massey-Woodward, R., Whalley, L., Forster, G., Bandy, B., 2018. ICOZA: Atmospheric species measurements of OH, HONO, HO2, NO, NO2, NOy, O3, SO2 and CO from Weybourne Atmosphere Observatory July 2015. Centre for Environmental Data Analysis. October 27, 2024. https://catalogue.ceda.ac.uk/uuid/ddf1032d626b45f78ce1c5e94f289a66/.

Dee, D.P., Uppala, S.M., Simmons, A.J., Berrisford, P., Poli, P., Kobayashi, S., Andrae, U., Balmaseda, M.A., Balsamo, G., Bauer, P., Bechtold, P., Beljaars, A.C.M., van de Berg, L., Bidlot, J., Bormann, N., Delsol, C., Dragani, R., Fuentes, M., Geer, A.J., Vitart, F., 2011. The ERA-interim reanalysis: Configuration and performance of the data assimilation system. Q. J. R. Meteorol. Soc. 137 (656), 553–597. https://doi.org/10.1002/qj.828.

DEFRA. (2017). Air Pollution in the UK 2016. *Annual Report 2016 Issue 2, September*, 131. https://uk-air.defra.gov.uk/assets/documents/annualreport/air_pollution_uk_2016_issue_1.pdf%0Ahttps://uk-air.defra.gov.uk/library/annualreport/viewonline?year=2016_issue_2.

Derwent, R.G., Manning, A.J., Simmonds, P.G., Spain, T.G., O'Doherty, S., 2018. Long-term trends in ozone in baseline and European regionally-polluted air at Mace head, Ireland over a 30-year period. Atmos. Environ. 179 (February), 279–287. https://doi.org/10.1016/j.atmosenv.2018.02.024.

Emmons, L.K., Hess, P.G., Lamarque, J.F., Pfister, G.G., 2012. Tagged ozone mechanism for MOZART-4, CAM-chem and other chemical transport models. Geosci. Model Dev. 5 (6), 1531–1542. https://doi.org/10.5194/gmd-5-1531-2012.

Entwistle, J., Weston, K., Singles, R., Burgess, R., 1997. The magnitude and extent of elevated ozone concentrations around the coasts of the British Isles. Atmos. Environ. 31 (13), 1925–1932. https://doi.org/10.1016/S1352-2310(97)00022-8.

Finch, D.P., Palmer, P.I., 2020. Increasing ambient surface ozone levels over the UK accompanied by fewer extreme events. Atmos. Environ. 237 (June), 117627. https://doi.org/10.1016/j.atmosenv.2020.117627.

Fischer, E.V., Jacob, D.J., Yantosca, R.M., Sulprizio, M.P., Millet, D.B., Mao, J., Paulot, F., Singh, H.B., Roiger, A., Ries, L., Talbot, R.W., Dzepina, K., Pandey Deolal, S., 2014. Atmospheric peroxyacetyl nitrate (PAN): A global budget and source attribution. Atmos. Chem. Phys. 14 (5), 2679–2698. https://doi.org/10.5194/acp-14-2679-2014.

Francis, X.V., Chemel, C., Sokhi, R.S., Norton, E.G., Ricketts, H.M.A., Fisher, B.E.A., 2011. Mechanisms responsible for the build-up of ozone over south East England during the august 2003 heatwave. Atmos. Environ. 45 (38), 6880–6890. https://doi.org/10.1016/j.atmosenv.2011.04.035.

Fuhrer, J., 2009. Ozone risk for crops and pastures in present and future climates. Naturwissenschaften 96 (2), 173–194. https://doi.org/10.1007/s00114-008-0468-7.

Garcia-Herrera, R., Díaz, J., Trigo, R. M., Luterbacher, J., & Fischer, E. M. (2010). A review of the european summer heat wave of 2003. In *critical reviews in environmental science and technology* (Vol. 40, issue 4, pp. 267–306). Taylor and Francis Inc. doi:https://doi.org/10.1080/10643380802238137.

Gouldsbrough, L., Hossaini, R., Eastoe, E., Young, P.J., 2022. A temperature dependent extreme value analysis of UK surface ozone. Atmos. Environ. 273 (October 2021), 1980–2019. https://doi.org/10.1016/j.atmosenv.2022.118975, 118975.

Grell, G.a., Peckham, S.E., Schmitz, R., McKeen, S.a., Frost, G., Skamarock, W.C., Eder, B., 2005. Fully coupled "online" chemistry within the WRF model. Atmos. Environ. 39 (37), 6957–6975. https://doi.org/10.1016/j.atmosenv.2005.04.027.

Grewe, V., Tsati, E., Mertens, M., Frömming, C., Jöckel, P., 2017. Contribution of emissions to concentrations: The TAGGING 1.0 submodel based on the modular earth submodel system (MESSy 2.52). Geosci. Model Dev. 10 (7), 2615–2633. https://doi.org/10.5194/gmd-10-2615-2017.

Grünhage, L., Pleijel, H., Mills, G., Bender, J., Danielsson, H., Lehmann, Y., Castell, J.F., Bethenod, O., 2012. Updated stomatal flux and flux-effect models for wheat for quantifying effects of ozone on grain yield, grain mass and protein yield. Environ. Pollut. 165, 147–157. https://doi.org/10.1016/j.envpol.2012.02.026.

Hoy, A., Hänsel, S., Skalak, P., & Bochnf, O. (2017). The extreme European summer of 2015 in a long-term perspective. 962(May 2016), 943–962. doi:https://doi.org/10.1002/joc.4751.

HTAP, 2007. Hemispheric Transport of Air Pollution 2007 Issue 17. https://doi.org/10.18356/2c908168-en.

Ionita, M., Tallaksen, L.M., Kingston, D.G., Stagge, J.H., Laaha, G., Lanen, H.A.J., Van, Scholz, P., Chelcea, S.M., Haslinger, K., 2017. The European 2015 drought from a climatological perspective, pp. 1397–1419. https://doi.org/10.5194/hess-21-1397-2017.

Jacob, D.J., Winner, D.A., 2009. Effect of climate change on air quality. Atmos. Environ. 43 (1), 51–63. https://doi.org/10.1016/j.atmosenv.2008.09.051.

Jenkin, M.E., Davies, T.J., Stedman, J.R., 2002. The origin and day of week dependence of photochemical ozone episodes in the UK. Atmos. Environ. 36 (6), 999–1012. https://doi.org/10.1016/S1352-2310(01)00360-0.

Kaser, L., Patton, E.G., Pfister, G.G., Weinheimer, A.J., Montzka, D.D., Flocke, F., Thompson, A.M., Stauffer, R.M., Halliday, H.S., 2017. The effect of entrainment through atmospheric boundary layer growth on observed and modeled surface ozone in the Colorado front range. J. Geophys. Res. 122 (11), 6075–6093. https://doi.org/10.1002/2016JD026245.

Kuenen, J., Dellaert, S., Visschedijk, A., Jalkanen, J.P., Super, I., Denier Van Der Gon, H., 2022. CAMS-REG-v4: a state-of-the-art high-resolution European emission inventory for air quality modelling. Earth System Science Data 14 (2), 491–515. https://doi.org/10.5194/essd-14-491-2022.

Kuenen, J.J.P., Visschedijk, a J.H., Jozwicka, M., Denier van der Gon, H.a.C., 2014. TNO-MACC_II emission inventory: a multi-year (2003–2009) consistent high-resolution European emission inventory for air quality modelling. Atmos. Chem. Phys. 14 (2013), 10963–10976. https://doi.org/10.5194/acpd-14-5837-2014.

Kuhn, L., Beirle, S., Kumar, V., Osipov, S., Pozzer, A., Bösch, T., Kumar, R., Wagner, T., 2024. On the influence of vertical mixing, boundary layer schemes, and temporal emission profiles on tropospheric NO2 in WRF-Chem - comparisons to in situ, satellite, and MAX-DOAS observations. Atmos. Chem. Phys. 24 (1), 185–217. https://doi.org/10.5194/acp-24-185-2024.

Lee, J.D., Lewis, A.C., Monks, P.S., Jacob, M., Hamilton, J.F., Hopkins, J.R., Watson, N. M., Saxton, J.E., Ennis, C., Carpenter, L.J., Carslaw, N., Fleming, Z., Bandy, B.J., Oram, D.E., Penkett, S.A., Slemr, J., Norton, E., Rickard, A.R., Whalley, K., L., … Jenkin, M. E., 2006. Ozone photochemistry and elevated isoprene during the UK heatwave of august 2003. Atmos. Environ. 40 (39), 7598–7613. https://doi.org/10.1016/j.atmosenv.2006.06.057.

Lee, J.D., Young, J.C., Read, K.A., Hamilton, J.F., Hopkins, J.R., Lewis, A.C., Bandy, B.J., Davey, J., Edwards, P., Ingham, T., Self, D.E., Smith, S.C., Pilling, M.J., Heard, D.E., 2009. Measurement and calculation of OH reactivity at a United Kingdom coastal site. J. Atmos. Chem. 64 (1), 53–76. https://doi.org/10.1007/s10874-010-9171-0.

Liu, X., Huey, L.G., Yokelson, R.J., Selimovic, V., Simpson, I.J., Müller, M., Jimenez, J.L., Campuzano-Jost, P., Beyersdorf, A.J., Blake, D.R., Butterfield, Z., Choi, Y., Crounse, J.D., Day, D.A., Diskin, G.S., Dubey, M.K., Fortner, E., Hanisco, T.F., Hu, W., Wolfe, G.M., 2017. Airborne measurements of western U.S. wildfire emissions: Comparison with prescribed burning and air quality implications. J. Geophys. Res. Atmos. 122 (11), 6108–6129. https://doi.org/10.1002/2016JD026315.

Lupaşcu, A., Butler, T., 2019. Source attribution of European surface O3 using a tagged O3 mechanism. Atmos. Chem. Phys. 19 (23), 14535–14558. https://doi.org/10.5194/acp-19-14535-2019.

Lupaşcu, A., Otero, N., Minkos, A., Butler, T., 2022. Attribution of surface ozone to NOx and volatile organic compound sources during two different high ozone events. Atmos. Chem. Phys. 22 (17), 11675–11699. https://doi.org/10.5194/acp-22-11675-2022.

Matsueda, M., 2011. Predictability of euro-Russian blocking in summer of 2010. Geophys. Res. Lett. 38 (6). https://doi.org/10.1029/2010GL046557.

Mertens, M., Kerkweg, A., Grewe, V., Jöckel, P., Sausen, R., 2020. Attributing ozone and its precursors to land transport emissions in Europe and Germany. Atmos. Chem. Phys. 20 (13), 7843–7873. https://doi.org/10.5194/acp-20-7843-2020.

Monks, P.S., 2005. Gas-phase radical chemistry in the troposphere. Chem. Soc. Rev. 34 (5), 376–395. https://doi.org/10.1039/b307982c.

Ordóñez, C., Barriopedro, D., Garciá-Herrera, R., Sousa, P.M., Schnell, J.L., 2017. Regional responses of surface ozone in Europe to the location of high-latitude blocks and subtropical ridges. Atmos. Chem. Phys. 17 (4), 3111–3131. https://doi.org/10.5194/acp-17-3111-2017.

Otero, N., Sillmann, J., Schnell, J.L., Rust, H.W., Butler, T., 2016. Synoptic and meteorological drivers of extreme ozone concentrations over Europe. Environ. Res. Lett. 11 (2), 024005. https://doi.org/10.1088/1748-9326/11/2/024005.

Otero, N., Jurado, O.E., Butler, T., Rust, H.W., 2022. The impact of atmospheric blocking on the compounding effect of ozone pollution and temperature: A copula-based approach. Atmos. Chem. Phys. 22 (3), 1905–1919. https://doi.org/10.5194/acp-22-1905-2022.

Penkett, S.A., Clemitshaw, K.C., Savage, N.H., Burgess, R.A., Cardenas, L.M., Carpenter, L.J., Mcfadyen, G.G., Cape, J.N., 1999. Studies of Oxidant Production at the Weybourne Atmospheric Observatory in Summer and Winter Conditions. 2, 111–128.

Pirovano, G., Balzarini, A., Bessagnet, B., Emery, C., Kallos, G., Meleux, F., Mitsakou, C., Nopmongcol, U., Riva, G.M., Yarwood, G., 2012. Investigating impacts of chemistry and transport model formulation on model performance at European scale. Atmos. Environ. 53, 93–109. https://doi.org/10.1016/j.atmosenv.2011.12.052.

Pope, R.J., Butt, E.W., Chipperfield, M.P., Doherty, R.M., Fenech, S., Schmidt, A., Arnold, S.R., Savage, N.H., 2016. The impact of synoptic weather on UK surface ozone and implications for premature mortality. Environ. Res. Lett. 11 (12). https://doi.org/10.1088/1748-9326/11/12/124004.

Porter, W.C., Heald, C.L., Cooley, D., Russell, B., 2015. Investigating the observed sensitivities of air-quality extremes to meteorological drivers via quantile regression. Atmos. Chem. Phys. 15 (18), 10349–10366. https://doi.org/10.5194/acp-15-10349-2015.

Powers, J. G., Klemp, J. B., Skamarock, W. C., Davis, C. A., Dudhia, J., Gill, D. O., Coen, J. L., Gochis, D. J., Ahmadov, R., Peckham, S. E., Grell, G. A., Michalakes, J., Trahan, S., Benjamin, S. G., Alexander, C. R., Dimego, G. J., Wang, W., Schwartz, C. S., Romine, G. S., … Duda, M. G. (2017). The weather research and forecasting model: Overview, system efforts, and future directions. Bull. Am. Meteorol. Soc., 98(8), 1717–1737. doi:https://doi.org/10.1175/BAMS-D-15-00308.1.

Pusede, S. E., Steiner, A. L., & Cohen, R. C. (2015). Temperature and recent trends in the chemistry of continental surface ozone. In Chemical Reviews (Vol. 115, Issue 10, pp. 3898–3918). American Chemical Society. doi:https://doi.org/10.1021/cr5006815.

Richmond-Bryant, J., Chris Owen, R., Graham, S., Snyder, M., McDow, S., Oakes, M., Kimbrough, S., 2017. Estimation of on-road NO2 concentrations, NO2/NOX ratios, and related roadway gradients from near-road monitoring data. Air Qual. Atmos. Health 10 (5), 611–625. https://doi.org/10.1007/s11869-016-0455-7.

Romero-Alvarez, J., Lupaşcu, A., Lowe, D., Badia, A., Archer-Nicholls, S., Dorling, S., Reeves, C.E., Butler, T., 2022. Sources of surface O3in the UK: Tagging O3within WRF-Chem. Atmos. Chem. Phys. 22 (20), 13797–13815. https://doi.org/10.5194/acp-22-13797-2022.

Rousi, E., Fink, A. H., Andersen, L. S., Becker, F. N., Beobide-arsuaga, G., Breil, M., Cozzi, G., Heinke, J., Jach, L., Niermann, D., Petrovic, D., & Richling, A. (2023). *The extremely hot and dry 2018 summer in central and northern Europe from a multi-faceted weather and climate perspective*. 1699–1718.

Russo, S., Sillmann, J., Fischer, E.M., 2015. Top Ten European Heatwaves since 1950 and their Occurrence in the Coming Decades Top Ten European Heatwaves since 1950 and their Occurrence in the Coming Decades.

Rustemeyer, N., Howells, M., 2021. ExcessMortality in England during the 2019 summer heatwaves. Climate 9 (1), 1–17. https://doi.org/10.3390/cli9010014.

Solberg, S., Hov, Søvde, A., Isaksen, I.S.A., Coddeville, P., De Backer, H., Forster, C., Orsolini, Y., Uhse, K., 2008. European surface ozone in the extreme summer 2003. J. Geophys. Res. Atmos. 113 (7), 1–16. https://doi.org/10.1029/2007JD009098.

Steele, C.J., Dorling, S.R., von Glasow, R., Bacon, J., 2014. Modelling Sea-Breeze Climatologies and Interactions on Coasts in the Southern North Sea: Implications for Offshore Wind Energy. Quarterly Journal of the Royal Meteorological Society, July, pp. 1821–1835. https://doi.org/10.1002/qj.2484.

Thompson, R., Landeg, O., Kar-Purkayastha, I., Hajat, S., Kovats, S., O'connell, E., 2022. Heatwave mortality in summer 2020 in England: an observational study. Int. J. Environ. Res. Public Health 19 (10). https://doi.org/10.3390/ijerph19106123.

Tuccella, P., Curci, G., Visconti, G., Bessagnet, B., Menut, L., Park, R.J., 2012. Modeling of gas and aerosol with WRF / Chem over Europe : Evaluation and sensitivity study. 117, 1–15. https://doi.org/10.1029/2011JD016302.

Gon, H.D., Der, Van, Hendriks, C., Kuenen, J., Seger, A., Visschedijk, A., 2011. *TNO Report Description of Current Temporal Emission Patterns and Sensitivity of Predicted AQ for Temporal Emission Patterns* (Issue December).

Vieno, M., Dore, A.J., Stevenson, D.S., Doherty, R., Heal, M.R., Reis, S., Hallsworth, S., Tarrason, L., Wind, P., Fowler, D., Simpson, D., Sutton, M.A., 2010. Modelling

surface ozone during the 2003 heat-wave in the UK. Atmos. Chem. Phys. 10 (16), 7963–7978. https://doi.org/10.5194/acp-10-7963-2010.
World Health Organization, 2016. Ambient air pollution: A global assessment of exposure and burden of disease. Clean Air J. 26 (2), 6–6.
Wong, J., 2013. Upper Tropospheric Ozone Enhancement during the North American Monsoon Evaluated Using the Weather Research and Forecasting Model with Chemistry (WRF-Chem).
Woodward-Massey, R., Sommariva, R., Whalley, L.K., Cryer, D.R., Ingham, T., Bloss, W. J., Ball, S.M., Cox, S., Lee, J.D., Reed, C.P., Crilley, L.R., Kramer, L.J., Bandy, B.J., Forster, G.L., Reeves, C.E., Monks, P.S., Heard, D.E., 2023. Radical chemistry and ozone production at a UK coastal receptor site. Atmos. Chem. Phys. 23 (22), 14393–14424. https://doi.org/10.5194/acp-23-14393-2023.